

Engineering Mesopore Formation in Hierarchical Zeolites under High Hydrostatic Pressure

Riku Sato,[#] Zhendong Liu,^{*#} Ce Peng, Che Tan, Peidong Hu, Jie Zhu, Masamori Takemura, Yasuo Yonezawa, Hiroki Yamada, Akira Endo, Javier García-Martínez, Tatsuya Okubo, and Toru Wakihara*



Cite This: <https://doi.org/10.1021/acs.chemmater.1c02800>



Read Online

ACCESS |



Metrics & More

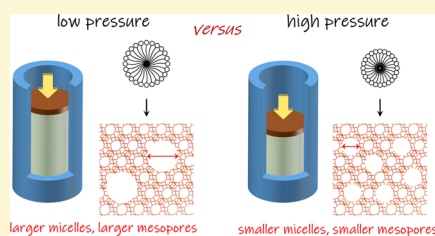


Article Recommendations



Supporting Information

ABSTRACT: Tailoring the textural properties of porous materials is of paramount importance to optimize their performance in a variety of applications. To this end, critical synthesis parameters influencing crystallization and reorganization of porous materials need to be identified and judiciously controlled. Although the effect of pressure on chemical transformations is ubiquitously present, its impact on fabricating porous materials with tailored physicochemical properties remains unexplored and its potential untapped. In this work, we disclose a detailed study on the effects of high hydrostatic pressure on the formation of well-controlled intracrystalline mesopores in ultrastable Y (USY) zeolite by the so-called surfactant-templating method. The rate of mesopore formation significantly increases upon elevating the pressure, whereas the average size of the mesopores—directed by the self-assembly of the surfactant—decreases. By simultaneously adjusting the external pressure and selecting surfactants of different lengths, we have been able to precisely control the mesopore size in the USY zeolite. Our findings clearly show that external hydrostatic pressure can be used to both accelerate mesopore formation and engineer their size with subnanometer precision. As a second example, we investigated the effect of external pressure on the synthesis of MCM-41. The results on MCM-41, consistent with our observations on the USY zeolite, further confirm that the use of high external pressure greatly affects the self-assembly behaviors of the amphiphilic molecules involved in the synthesis/modification of the porous materials. Our results show that the high-pressure approach represents an untapped opportunity for synthesis/modification of functional porous materials that will likely yield new discoveries in this field.



INTRODUCTION

Pressure is a critical parameter to chemical reactions, as it governs both thermodynamic and kinetics aspects.¹ According to the van't Hoff equation, elevating pressure favors the equilibrium to move forward for a reaction with a negative reaction volume.² For a long time, this principle has often been practiced in gas-phase reactions, such as ammonia synthesis and production of polyethylene. Upon high pressure, geometrical confinements can be generated to molecules in the liquid and solid phases, which alter the electronic structures of molecules, modulate intermolecular interactions, and change the overall free energy landscape.³ These high-pressure effects lead to reaction outcomes that could not be possible at ambient pressure, such as artificial syntheses of diamond and boron nitride.⁴ Most of the high-pressure syntheses involve dense crystals where atoms are arranged in close-packed symmetries. Few studies have been targeted at open framework materials, which are a class of materials featuring ordered inorganic or hybrid structures that form nanosized pores, channels, and cages. Representative open framework materials include zeolites, mesoporous oxides, and metal-organic frameworks (MOFs).⁵ Tailoring physicochemical properties of open framework materials is of paramount importance to

optimize their performance in diverse applications. In particular, precise pore engineering is of great significance, as many functions of the open framework materials rely on mechanisms of size recognition or confinement effect, which requires size regulation with high accuracy and over a broad spectrum.^{6,7} A number of factors, such as selection of organic templates or ligands, synthesis conditions, and postsynthesis activation/modification procedures, are widely used to influence the pore characteristics of the open framework materials.⁸ However, pressure is not considered among these parameters, which renders its impact underestimated and its potential untapped.

Zeolites are a class of open frameworks built upon tetrahedral silicon and aluminum oxides.^{9,10} Owing to their high stability, unique pore architecture, and adjustable acidity, zeolites have been widely used in a variety of chemical

Received: August 13, 2021

Revised: October 1, 2021

63 processes.^{11–13} To further improve the performance of zeolites
64 in those applications, both hydrothermal synthesis (“bottom-
65 up” approach) and postsynthesis modification (“top-down”
66 approach) have been studied in great detail. The crystallization
67 of zeolites is very sensitive to conditions where hydrothermal
68 synthesis is carried out.^{14–16} Recently, we reported the effects
69 of high external pressure on the hydrothermal synthesis of
70 zeolites from alkali-metal-containing aluminosilicate precursors
71 without the addition of any organic molecules, where unique
72 crystallization behaviors contradicting the observations under
73 autogenous pressures were revealed.¹⁷ Organic molecules have
74 played an important role in the synthesis and postsynthesis
75 modification of zeolites. For example, organic molecules have
76 been extensively employed as structure-directing agents for
77 synthesizing zeolites,^{18–20} as crystal growth modifiers for
78 tuning the bulky morphology of zeolites,^{21,22} and as
79 mesoporegens for creating hierarchical zeolites.²³ Applying
80 high external pressure during both the synthesis and
81 postsynthesis modification of zeolites in the presence of
82 organic compounds is expected to offer untapped oppor-
83 tunities.

84 Herein, we report the use of surfactants under high external
85 pressure to introduce tunable mesoporosity in ultrastable Y
86 (USY) zeolite and porous silica and provide new insights into
87 organic–inorganic interactions that determine the pore size
88 and architecture of the templated materials. We first present a
89 systematic study on the effect of high hydrostatic pressure on
90 the surfactant templating of the USY zeolite. The surfactant-
91 templating process is a well-known postsynthetic strategy that
92 allows for introducing large amounts of tunable mesoporosity
93 in zeolites while preserving their most important properties.
94 The mesopores generated by this method have an average pore
95 size corresponding to the micelle size.^{24–26} This feature allows
96 us to reveal how the assembly of the surfactant molecules to
97 form micelles evolves in response to high external pressures
98 and consequently alters the mesopore size of the zeolite. To
99 gain additional insights into the impact of high pressure on the
100 packing behavior of the surfactants and the size of the
101 mesopores produced by micelles, we carried out a second
102 study, in which we focused on the synthesis of ordered
103 mesoporous silica MCM-41, which further confirmed our
104 conclusions. Because the size of its mesopores is determined by
105 the size of the micelles used to prepare it,²⁷ the study on
106 MCM-41 provides a fundamental and simple method to study
107 the role of external pressure on the micelle size and therefore
108 on the mesopore size of the surfactant-templated USY zeolite.

109 ■ EXPERIMENTAL SECTION

110 **Materials.** CBV720 (USY) was provided by Zeolyst with a Si/Al
111 ratio of 15. Sodium hydroxide (NaOH), octyltrimethylammonium
112 bromide, dodecyltrimethylammonium bromide, tetradecyltrimethy-
113 lammonium bromide, cetyltrimethylammonium bromide (CTAB),
114 and octadecyltrimethylammonium bromide were purchased from
115 Wako Pure Chemical Industries (Ltd.). All chemicals were used
116 without further purification. Deionized water was used in all
117 experiments.

118 **Apparatus.** A homemade warm isostatic press (WIP, see Figure
119 S1) was used as the pressurization apparatus, and deionized water was
120 used as the pressure medium. The maximum treatment temperature
121 was 150 °C, and the pressure was 200 MPa. A Teflon tube was
122 purchased from MISUMI and used as the reaction vessel (see Figure
123 S2). The Teflon tube was heat-sealed at 330 °C at both ends, which
124 were further sealed with metal clips. The sealed Teflon tube was then
125 placed in the chamber of the WIP.

Surfactant Templating of the USY Zeolite. In a typical run, 126
0.09 g of CTAB was dissolved in 3.42 g of NaOH solution (0.49 wt
127 %) followed by stirring for 30 min. Thereafter, 0.18 g of parent zeolite
128 (Zeolyst CBV720, Si/Al ratio of 15) was added, giving a mixture with
129 a molar ratio of 1 TO₂:0.082 CTAB:0.14 NaOH:75 H₂O (TO₂
130 represents SiO₂ and 1/2Al₂O₃). Subsequently, the mixture was sealed
131 in a Teflon vessel and then placed in a high-pressure treatment
132 apparatus. The treatment was performed at a certain temperature
133 (50–150 °C) for 30 min to 120 h under different pressures from
134 autogenous pressure to 200 MPa. After the treatment, the product
135 was washed with deionized water and recovered by centrifugation and
136 drying. The recovered zeolites were calcined at 550 °C for 5 h in a
137 muffle oven. 138

Synthesis of MCM-41. In the synthesis under autogenous
139 pressure, CTAB (0.8 g) was dissolved in a NaOH aqueous solution
140 (0.1 M, 42.8 mL), which was vigorously stirred at 40 °C for 20 min.
141 Thereafter, tetraethyl orthosilicate (TEOS, 3.81 g) was added
142 dropwise to the previous solution. The resultant white slurry was
143 first stirred at 40 °C for 2 h and then heated at 100 °C for 24 h. The
144 solid precipitates were recovered by vacuum filtration, washed with
145 deionized water, and dried at 80 °C before calcination at 550 °C for 5
146 h to remove the organic template. In the synthesis under 200 MPa,
147 the abovementioned white slurry was sealed in the Teflon vessel and
148 then placed in the WIP for the synthesis for 24 h at 100 °C. The high-
149 pressure product was recovered, washed, dried, and calcined as per
150 the same procedure. 151

Characterization. Powder X-ray diffraction (XRD) patterns of all
152 samples were obtained using a Rigaku Ultima IV diffractometer with
153 Cu K α radiation ($\lambda = 1.5406 \text{ \AA}$, $V = 40 \text{ kV}$, $I = 40 \text{ mA}$) at a scanning
154 rate of 4° min⁻¹. The product morphology was observed using a field
155 emission scanning electron microscope (FE-SEM, JSM-7000F, JEOL,
156 Japan). Transmission electron microscopy (TEM) images were taken
157 on a JEM-2000EX (JEOL, Japan) under a working voltage of 120 kV.
158 Nitrogen adsorption–desorption isotherms were obtained on a
159 Quantachrome Autosorb-iQ2 instrument at liquid nitrogen temper-
160 ature with an outgas pretreatment at 325 °C for 4 h under vacuum.
161 Mesopore volume (V_{meso}) was calculated based on the nonlinear
162 density functional theory (NLDFT) method using the adsorption
163 branch of the N₂ adsorption–desorption isotherms.^{28,29} Elemental
164 analysis was performed on a Thermo iCAP 6300 inductively coupled
165 plasma-atomic emission spectrometer (ICP-AES). Thermogravimetric
166 and differential thermal analysis (TG–DTA) was conducted on a
167 Rigaku PU 4K from 30 to 800 °C at a heating rate of 10 °C min⁻¹
168 with a flow of 10 vol % O₂ and 90 vol % He mixed gas. The cross-
169 sectional features of the samples were observed using a field emission
170 scanning electron microscope (SU9000, Hitachi). Prior to the
171 observation, the zeolite powders embedded in epoxy resin were cut
172 and polished using a broad Ar⁺ ion beam in a cross section polisher
173 (E-3500, Hitachi). 174

175 ■ RESULTS AND DISCUSSION

176 **Figure 1A** shows the XRD patterns of the pristine USY zeolite
177 and those surfactant-templated at 100 °C for 30 min under
178 different pressures. All of the samples are highly crystalline,
179 even those surfactant-templated at elevated external pressures,
180 as indicated by the XRD patterns. Meanwhile, there was no
181 remarkable change in the Si/Al ratio (Si/Al ratios all around
182 15) and weight loss after the treatment, which is consistent
183 with the observations in previous studies.^{24–26} The bulk
184 morphology of the USY zeolite did not change after the
185 surfactant templating (Figure S3). The crystal lattices of the
186 USY zeolites surfactant-templated under different pressures did
187 not change, as evidenced by the unchanged positions of the
188 XRD peaks shown in Figure 1A. A broad low-angle XRD peak
189 centered at approximately 2° appeared after the treatment, due
190 to the presence of the surfactant-templated mesopores. The
191 surfactant-templated zeolite featured tortuous mesopores, and
192 therefore, the broad peak developed in the low-angle range of 192

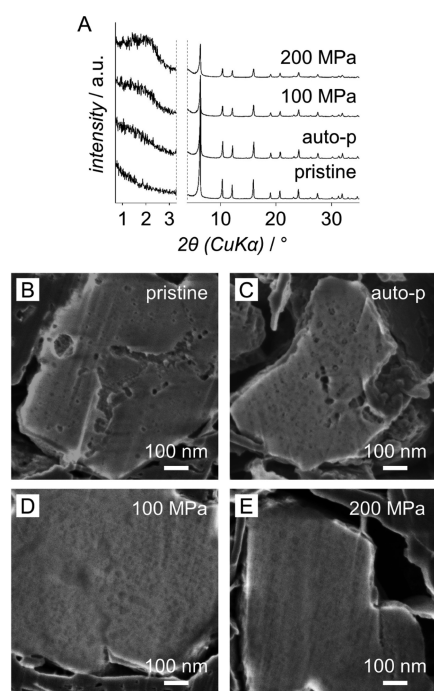


Figure 1. Surfactant templating of the USY zeolite under different pressures. (A) XRD patterns of pristine USY and those surfactant-templated in a CTAB-containing NaOH solution at 100 °C for 30 min under different pressures. (B) Cross-sectional SEM image of pristine USY. (C–E) Cross-sectional SEM images of the USY zeolites surfactant-templated under autogenous pressure, 100, and 200 MPa, respectively.

193 the XRD pattern.³⁰ The intensity of this peak increased with
 194 the external pressure applied, suggesting that at higher
 195 pressures, the mesopores were better ordered. To confirm
 196 this point, we examined the cross sections of the samples by a
 197 scanning electron microscope (SEM) before and after the
 198 treatment. Figure 1B shows that the pristine USY zeolite had
 199 large mesopores that were generated by steaming. Figure 1C–
 200 E depicts that the evolution from the initially large mesopores
 201 to smaller mesopores, which reveals a pressure-dependent
 202 tendency. The large mesopores, which were generated by
 203 steaming in the manufacture of USY, are the most prevalent
 204 after the treatment under autogenous pressure; however, when

high external pressure was applied, considerable amounts of
 205 smaller mesopores are observed. In particular, the sample
 206 surfactant-templated at 200 MPa exhibited the highest amount
 207 of smaller mesopores, which is consistent with the XRD
 208 patterns shown in Figure 1A. These mesopores were much
 209 uniform and of smaller size, which renders the cross section of
 210 the surfactant-templated USY to possess fine texture
 211 (particularly, as depicted by the SEM image in Figure 1E).
 212 This observation was further confirmed by the transmission
 213 electron microscopy (TEM) images and by measuring the
 214 amount of CTAB occluded in the zeolites (see Figures S4 and
 215 S5, respectively, for more details). Collectively considering all
 216 these results, we concluded that the surfactant templating of
 217 the USY zeolite can be accelerated by applying external
 218 pressure.

Figure 2A–C shows the pore size distributions of pristine
 220 USY and those surfactant-templated for different periods of
 221 time under autogenous pressure, 100, and 200 MPa,
 222 respectively. The pore size distributions were derived from
 223 the adsorption branch of the N₂ adsorption–desorption
 224 isotherms (see Figure S6) at 77 K using a nonlinear density
 225 functional theory model (NLDFT model).^{28,29} Pristine USY
 226 features a low amount of mesopores in the 2–8 nm
 227 (pore width) and a broad pore size distribution. As a result of
 228 surfactant templating in the CTAB-containing NaOH solution,
 229 the number of mesopores gradually increased with time and
 230 the pore size distribution became narrower. These results
 231 further confirm that the surfactant templating of USY
 232 proceeded much faster under high external pressures than
 233 under autogenous pressure. Meanwhile, the pore size
 234 distribution of the USY zeolites surfactant-templated under
 235 high pressures becomes narrower. Table S1 shows the data of
 236 the mesopore volume of the samples, which included only the
 237 newly formed mesopores sized in the range of 2–8 nm. The
 238 pristine USY zeolite contained mesopores in a broader size
 239 distribution, but only a moderate amount of mesoporosity in
 240 the range of 2–8 nm. After surfactant templating, uniform
 241 mesopores developed apparently, amounting to mesopore
 242 volumes higher than 0.35 cm³ g⁻¹. Again, this result
 243 demonstrates that high external pressure prompted pore
 244 reconstruction, resulting in a faster increase of uniform
 245 mesopores.

As described elsewhere,^{24–26} the surfactant-templating
 247 process involves the following steps: (1) cleavage of the Si–
 248

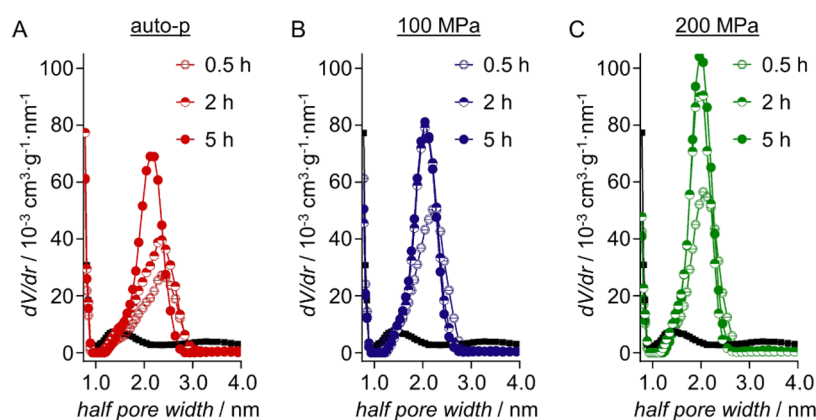


Figure 2. Time evolution of the pore size distributions of the mesoporous USY zeolites surfactant-templated under different pressures. (A–C) Pore size distributions of the USY zeolites treated over different periods of time under autogenous pressure, 100, and 200 MPa, respectively. (The temperature for surfactant templating was 100 °C. The black curve represents the pore size distribution of the pristine USY zeolite.)

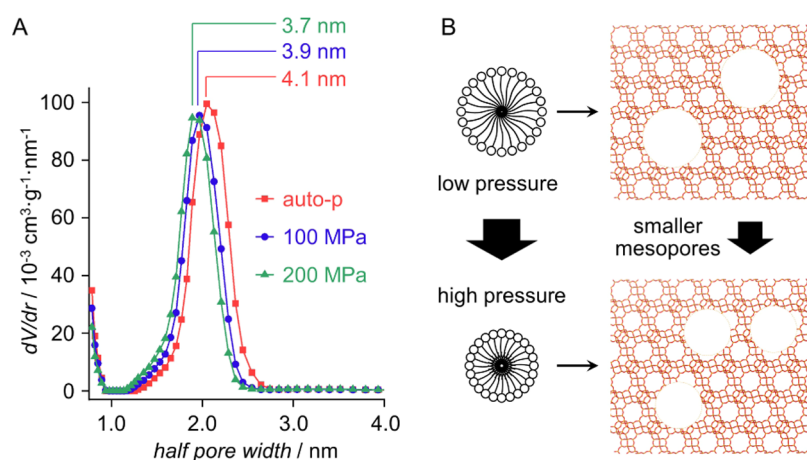


Figure 3. Effect of pressure on the average mesopore size of the surfactant-templated USY zeolite. (A) Comparison of the pore size distributions of the surfactant-templated USY zeolites with CTAB obtained under different pressures. (B) Schematic illustration of the effect of high external pressure on micelle size and corresponding mesopore size. (In all cases, the surfactant templating was performed at 100 °C for 120 h.)

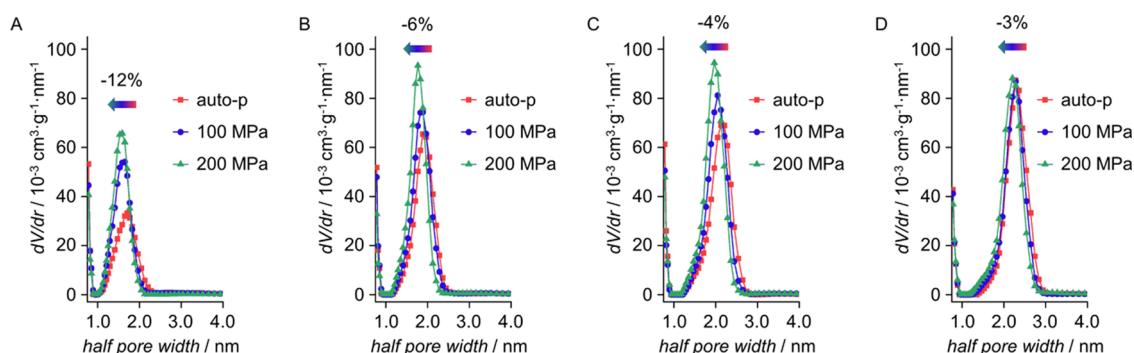


Figure 4. Reduction of mesopore size as a function of external pressure applied during the surfactant templating of the USY zeolite with surfactants of different carbon chain lengths. (A–D) Pore size distributions of the surfactant-templated USY zeolites obtained under different pressures with four trimethylalkylammonium surfactants ($C_nH_{2n+1}N^+(CH_3)_3$, $n = 12, 14, 16,$ and 18 , from left to right). (In all of the cases, the surfactant templating was performed at 100 °C for 5 h.)

249 O–Si bond with the assistance of OH^- ions, which generates
 250 abundant Si–O $^-$ sites; (2) admission of CTA $^+$ cations inside
 251 the zeolite driven by the presence of the Si–O $^-$ sites via
 252 electrostatic interaction; and (3) formation of well-defined
 253 mesopores produced by the micelles that form inside the
 254 zeolite where the local concentration of the CTA $^+$ is high
 255 enough. Exerting high pressure on substances in the liquid
 256 phase increases their density and reduces the intermolecular
 257 distance, which enhances the frequency of collision between
 258 molecules.^{2,3} Meanwhile, the solubility of electrolytes could be
 259 increased in a pressurized aqueous medium.^{31,32} As a result of
 260 the increased solubility, the external high pressure facilitates
 261 the cleavage of the Si–O–Si bonds under the alkaline
 262 condition to form the Si–O $^-$ terminal groups, needed for
 263 the surfactant templating of the zeolite. In the absence of
 264 CTAB, the high-silica zeolite tends to dissolve into the alkaline
 265 solution, resulting in structural collapse. Under high pressure,
 266 faster dissolution of the USY zeolite was observed, which led to
 267 the collapse of its micropore system in just 30 min (Figure S7),
 268 an observation that confirms the abovementioned claim of the
 269 accelerated cleavage of the Si–O–Si bonds by NaOH under
 270 high external pressure. Furthermore, the external high pressure
 271 could possibly accelerate the micellization of the CTA $^+$ inside
 272 the USY zeolite, which is a key step in the formation of the
 273 smaller mesopores. For the above reasons, we conclude that
 274 high external pressure can be used to accelerate the cascade of

steps involved in the surfactant templating of the USY zeolite,
 leading to the faster formation of uniform mesopores. The
 enhancement of mesopore formation upon high pressure is
 consistent with our previous study, in which applying high
 external pressures was found to greatly prompt the
 crystallization of zeolites from sodium- and potassium-
 containing aluminosilicate precursors.¹⁷ It is worth noting
 that the enhancement effect of high external pressure was more
 pronounced at a higher temperature, as indicated by the results
 in Figure S8, which is expected due to the role of temperature
 in overcoming the low activation energy involved in the
 surfactant templating of the USY zeolite.²⁵ These results
 collectively demonstrate that the pressure effect is significant
 and can be exploited to accelerate the rates of both synthesis
 and modification of zeolites.

Besides accelerating the rate of surfactant templating, the
 external high pressure was found to alter the size of the
 mesopores. Figure 3A compares the pore size distributions of
 the USY zeolite surfactant-templated under different pressures.
 The corresponding N_2 adsorption–desorption isotherms are
 shown in Figure S9. To avoid the influence of synthesis time,
 the samples were subject to the treatments for enough long
 period of time (120 h). Under autogenous pressure, an average
 pore size of 4.10 nm was obtained, which is in accordance with
 the size of CTAB micelles, as discussed in previous
 studies.^{24–26} In contrast, the average pore sizes for the samples

301 treated at 100 and 200 MPa were 3.9 and 3.7 nm, respectively,
302 showing that the mesopores shrunk upon the external high
303 pressures.

304 A key feature of the surfactant templating of zeolites is that
305 the size of the mesopores is governed by the assembly of the
306 surfactants. The above result suggests that the high external
307 pressure contracts the micelle size of the surfactants, which
308 conveys to the surfactant templating of the USY zeolite and
309 consequently results in a smaller mesopores size (Figure 3B).
310 As CTAB contains long aliphatic chain alkanes, smaller
311 micelles should be expected in a highly pressurized environ-
312 ment, as discussed in previous studies.^{33,34}

313 To further reveal the effect of high external pressure on the
314 assembly of surfactants and thereof the mesopore size of the
315 surfactant-templated USY zeolite, trimethylalkylammonium
316 surfactants with different carbon chain lengths
317 ($C_nH_{2n+1}N^+(CH_3)_3$, $n = 12, 14, 16$, and 18) were studied. As
318 seen from the results under autogenous pressure (Figure S10),
319 there exists a linear relationship between the carbon number of
320 the alkane chain and the average mesopore size of the
321 surfactant-templated USY zeolite. Figure S11 shows the N_2
322 adsorption–desorption isotherms of the samples surfactant-
323 templated with surfactants having different carbon chain
324 lengths. Figure 4 shows the comparisons of pore size
325 distributions under different pressures for the four trimethy-
326 lalkylammonium surfactants. In all cases, the average pore size
327 decreased with pressure. It is worth noting that the smaller the
328 surfactant, the more pronounced the reduction in the
329 mesopore size with pressure. According to previous studies,
330 the number of molecules present in a micelle (known as the
331 aggregation number) is smaller for a surfactant with shorter
332 aliphatic chains.^{35,36} A smaller aggregation number also results
333 in a larger void in the micelles, which could explain why the
334 mesopores size reduction at high pressures is more notable for
335 smaller surfactant molecules. On the other hand, smaller
336 surfactants display weaker hydrophobic attraction in the
337 micelle, making its shrinkage more favorable at high external
338 pressures. Table S2 presents average pore sizes and mesopore
339 volumes of the surfactant-templated zeolites under different
340 pressures. In all cases, a high mesopore volume was achieved
341 ($>0.25 \text{ cm}^3 \text{ g}^{-1}$), which indicates that the conditions used were
342 sufficient to surfactant template the zeolite. More importantly,
343 fine control over the mesopore size ranging from ca. 3.2 nm
344 (small surfactant and high pressure) to ca. 4.6 nm (large
345 surfactant and autogenous pressure) was achieved. As many
346 applications of zeolites are enabled via mechanisms of size
347 recognition and spatial confinement, it is particularly important
348 for us to be able to regulate the pore size of zeolites with high
349 precision (in an increase of 0.1 Å) and over a wide spectrum
350 (from the size of small molecules to that of large ones). For
351 example, the separation of ethylene and ethane through
352 molecular sieving requires precise tailoring of the pore size of
353 the porous medium, considering the fact that the kinetic
354 diameters of the two molecules only differ marginally (by 0.28
355 Å).⁶ When bulky reactants or transition states are in a “right
356 fit” with the pores or voids of the zeolite catalysts, the
357 confinement effect can be generated and thus enhance the
358 catalytic performance,⁷ which pinpoints the importance of
359 fabricating catalysts with specific size and geometry. These
360 prospects have stimulated considerable efforts in innovating
361 synthesis methods to tailor the pore features of zeolites (and
362 other porous materials). As demonstrated by the above results,
363 the combination of judiciously applying external pressure and

appropriately selecting surfactants offered a unique oppor- 364
tunity to tune the mesopore size in the hierarchical USY zeolite 365
with high precision. Thus, we believe that the high-pressure 366
synthesis/modification offers a new method and enriches the 367
toolbox for engineering the pore features of porous materials. 368

To confirm the impact of high pressure on the shrinkage of 369
the micelles and ultimately on the reduction of the mesopore 370
size of the hierarchical zeolites, we extended our investigation 371
to a well-known surfactant-templated material—mesoporous 372
silica MCM-41. MCM-41 features hexagonally arranged one- 373
dimensional mesopores. It is the best-known and most studied 374
member of the M41S family, a series of ordered mesoporous 375
silica synthesized from quaternary-ammonium-based surfac- 376
tants.^{37,38} Thanks to the extensive knowledge gained over the 377
past few decades, the architecture of the mesopores 378
(hexagonal, cubic, or lamellar) of the M41S materials can be 379
controlled by selecting surfactants of different packing factors 380
(g -factor).²⁷ Not only the mesopore architecture but also the 381
mesopore size of MCM-41 can be finely tuned by choosing an 382
appropriate surfactant in combination with adopting the right 383
synthesis condition. Because of these features, the synthesis of 384
MCM-41 serves as an excellent model material to study the 385
impact of high pressure on the surfactant templating. Figure 5A 386

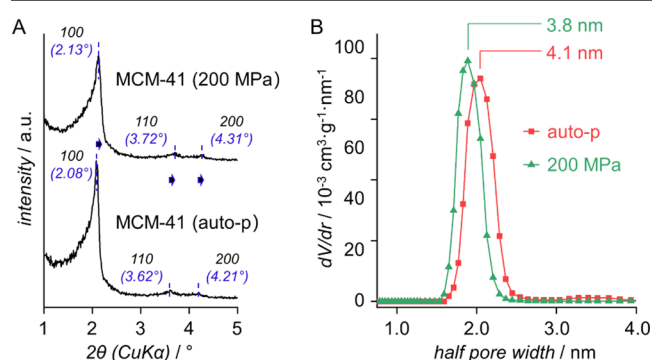


Figure 5. Comparison of the syntheses of MCM-41 under autogenous pressure and 200 MPa. (A) XRD patterns of the MCM-41 samples (the arrows indicate peak shifts toward higher 2θ angles). (B) Pore size distributions of the MCM-41 samples.

shows the XRD patterns of the samples synthesized under 387
autogenous pressure and 200 MPa, from which main reflection 388
lines (d_{100} , d_{110} , and d_{200}) of the hexagonal symmetry of the 389
MCM-41 structure (space group: $p6m$) are observed.²⁷ It is 390
worth noting that the high-pressure MCM-41 exhibited XRD 391
peaks that shift to higher 2θ angles compared to the other one, 392
implying that it may contain smaller mesopores. Figure S12 393
shows the SEM and TEM images of the samples, which 394
together with high Brunauer–Emmett–Teller (BET) surface 395
areas (920 and $880 \text{ m}^2 \text{ g}^{-1}$ for the samples synthesized under 396
autogenous pressure and 200 MPa, respectively) displayed in 397
Figure S13 further confirm that MCM-41 was successfully 398
synthesized. The pore size distributions calculated from the N_2 399
adsorption data (Figure 5B) show that the average mesopore 400
size of the high-pressure MCM-41 (3.7 nm) is smaller than 401
that of the one synthesized under autogenous pressure (4.1 402
nm). This result, significantly consistent with the observations 403
on the surfactant templating of the USY zeolite with CTAB, 404
further validates that high external pressure can be used to 405
affect the self-assembly behaviors of the surfactants and thus 406
alter the pore dimensions of the templated materials. From the 407

408 corresponding d100 reflections in shown Figure 5A, the
409 distances between two mesopore centers in the MCM-41
410 samples synthesized under autogenous pressure and 200 MPa
411 were calculated to be 4.9 and 4.8 nm, respectively. Thus, the
412 wall thickness was estimated to be 0.8 nm for the autogenous-
413 pressure MCM-41 and 1.1 nm for the high-pressure MCM-41.
414 This result suggests that, along with shrinking the mesopores,
415 high external pressures yield MCM-41 with a thick wall and
416 likely higher structural stability.^{39,40}

417 ■ CONCLUSIONS

418 In this work, we show how high hydrostatic pressure can be
419 utilized to engineer mesopores in the hierarchical USY zeolite
420 and MCM-41. High external pressure accelerates the cascade
421 of processes responsible for the surfactant templating of the
422 USY zeolite and thus leads to a significantly faster generation
423 of mesopores. Moreover, high external pressure influences the
424 assembly behavior of surfactants; thus, it can be utilized to
425 regulate the micelle size and consequently engineer the
426 mesopore sizes, with subnanometer precision, of the templated
427 USY zeolite and MCM-41. Applying high pressure also yields
428 narrower pore size distributions in templated materials and
429 thickens the pore walls of MCM-41. These results collectively
430 show that high external pressure enriches our toolbox to
431 influence the self-assembly behavior, which is critically
432 important to engineer the porosity of open framework
433 materials. We anticipate that this work will stimulate future
434 studies to exploit the high-pressure synthesis of functional
435 porous materials as well as to gain deeper insights into the
436 processes involved.

437 ■ ASSOCIATED CONTENT

438 **SI** Supporting Information

439 The Supporting Information is available free of charge at
440 <https://pubs.acs.org/doi/10.1021/acs.chemmater.1c02800>.

441 Supporting tables; illustration and photograph of the
442 WIP; N₂ adsorption–desorption isotherms; and SEM
443 and TEM images (PDF)

444 ■ AUTHOR INFORMATION

445 Corresponding Authors

446 **Zhendong Liu** – Department of Chemical System Engineering,
447 The University of Tokyo, Tokyo 113-8656, Japan; Institute of
448 Engineering Innovation, The University of Tokyo, Tokyo 113-
449 8656, Japan; Present Address: State Key Laboratory of
450 Chemical Engineering, Department of Chemical
451 Engineering, Tsinghua University, Beijing 100084, China;
452 orcid.org/0000-0002-3364-2523; Email: [liuzd@](mailto:liuzd@tsinghua.edu.cn)
453 [tsinghua.edu.cn](mailto:liuzd@tsinghua.edu.cn)

454 **Toru Wakihara** – Department of Chemical System
455 Engineering, The University of Tokyo, Tokyo 113-8656,
456 Japan; Institute of Engineering Innovation, The University of
457 Tokyo, Tokyo 113-8656, Japan; orcid.org/0000-0002-3916-3849; Email: wakihara@chemsys.t.u-tokyo.ac.jp

459 Authors

460 **Riku Sato** – Department of Chemical System Engineering, The
461 University of Tokyo, Tokyo 113-8656, Japan

462 **Ce Peng** – Department of Chemical System Engineering, The
463 University of Tokyo, Tokyo 113-8656, Japan

464 **Che Tan** – Department of Chemical System Engineering, The
465 University of Tokyo, Tokyo 113-8656, Japan

Peidong Hu – Department of Chemical System Engineering, 466
The University of Tokyo, Tokyo 113-8656, Japan 467

Jie Zhu – Department of Chemical System Engineering, The 468
University of Tokyo, Tokyo 113-8656, Japan 469

Masamori Takemura – Department of Chemical System 470
Engineering, The University of Tokyo, Tokyo 113-8656, 471
Japan 472

Yasuo Yonezawa – Department of Chemical System 473
Engineering, The University of Tokyo, Tokyo 113-8656, 474
Japan 475

Hiroki Yamada – Research Institute for Chemical Process 476
Technology, National Institute of Advanced Industrial Science 477
and Technology, Tsukuba, Ibaraki 305-8565, Japan; SPring- 478
8, Japan Synchrotron Radiation Research Institute (JASRI), 479
Sayo-gun, Hyogo 679-5198, Japan 480

Akira Endo – Research Institute for Chemical Process 481
Technology, National Institute of Advanced Industrial Science 482
and Technology, Tsukuba, Ibaraki 305-8565, Japan 483

Javier García-Martínez – Laboratorio de Nanotecnología 484
Molecular, Departamento de Química Inorgánica, 485
Universidad de Alicante, Alicante 03690, Spain; 486
orcid.org/0000-0002-7089-4973 487

Tatsuya Okubo – Department of Chemical System 488
Engineering, The University of Tokyo, Tokyo 113-8656, 489
Japan; orcid.org/0000-0002-1681-0193 490

Complete contact information is available at: 491

<https://pubs.acs.org/doi/10.1021/acs.chemmater.1c02800> 492

493 Author Contributions

#R.S. and Z.L. contributed equally to this work. 494

495 Notes

The authors declare no competing financial interest. 496

497 ■ ACKNOWLEDGMENTS

Z.L. thanks the Japan Society for the Promotion of Science 498
(JSPS) for financial support (a Grant-in-Aid for Young 499
Scientists: 18K14049). This work was partly supported by 500
New Energy and Industrial Technology Development 501
Organization (NEDO) under Moonshot Project, the Japan 502
Society for the Promotion of Science (JSPS), KAKENHI 503
Grant-in-Aid for Transformative Research Areas (A) 504
JP20A206/20H05880, and the Materials Processing Science 505
project (“Mater realize”) of MEXT, Grant Number 506
JPMXP0219192801. J.G.-M. acknowledges funding from the 507
European Commission through the H2020-MSCA-RISE-2019 508
program (ZEOBIOCHEM—872102) and the Spanish MI- 509
CINN and AEI/FEDER (RTI2018-099504-B-C21). 510

511 ■ REFERENCES

- (1) Schettino, V.; Bini, R. Constraining molecules at the closest 512
approach: chemistry at high pressure. *Chem. Soc. Rev.* **2007**, *36*, 869– 513
880. 514
- (2) Mugnai, M.; Pagliai, M.; Cardini, G.; Schettino, V. Mechanism of 515
the ethylene polymerization at very high pressure. *J. Chem. Theory* 516
Comput. **2008**, *4*, 646–651. 517
- (3) Chen, B.; Hoffmann, R.; Cammi, R. The Effect of pressure on 518
organic reactions in fluids—a new theoretical perspective. *Angew.* 519
Chem., Int. Ed. **2017**, *56*, 11126–11142. 520
- (4) Haines, J.; Léger, J.; Bocquillon, G. Synthesis and design of 521
superhard materials. *Annu. Rev. Mater. Res.* **2001**, *31*, 1–23. 522
- (5) Liu, Z.; Zhu, J.; Peng, C.; Wakihara, T.; Okubo, T. Continuous 523
flow synthesis of ordered porous materials: from zeolites to metal– 524

- 525 organic frameworks and mesoporous silica. *React. Chem. Eng.* **2019**, *4*,
526 1699–1720.
- 527 (6) Liu, Y.; Wu, Y.; Liang, W.; Peng, J.; Li, Z.; Wang, H.; Janik, M. J.;
528 Xiao, J. Bimetallic ions regulate pore size and chemistry of zeolites for
529 selective adsorption of ethylene from ethane. *Chem. Eng. Sci.* **2020**,
530 *220*, No. 115636.
- 531 (7) Gounder, R.; Iglesia, E. The roles of entropy and enthalpy in
532 stabilizing ion-pairs at transition states in zeolite acid catalysis. *Acc.*
533 *Chem. Res.* **2012**, *45*, 229–238.
- 534 (8) Slater, A. G.; Cooper, A. I. Function-led design of new porous
535 materials. *Science* **2015**, *348*, No. aaa8075.
- 536 (9) Davis, M. E.; Lobo, R. F. Zeolite and molecular sieve synthesis.
537 *Chem. Mater.* **1992**, *4*, 756–768.
- 538 (10) Davis, M. E. Ordered porous materials for emerging
539 applications. *Nature* **2002**, *417*, 813–821.
- 540 (11) Corma, A. From microporous to mesoporous molecular sieve
541 materials and their use in catalysis. *Chem. Rev.* **1997**, *97*, 2373–2420.
- 542 (12) Tsapatsis, M. Molecular sieves in the nanotechnology era.
543 *AIChE J.* **2002**, *48*, 654–660.
- 544 (13) Primo, A.; Garcia, H. Zeolites as catalysts in oil refining. *Chem.*
545 *Soc. Rev.* **2014**, *43*, 7548–7561.
- 546 (14) Wakihara, T.; Okubo, T. Hydrothermal synthesis and
547 characterization of zeolites. *Chem. Lett.* **2005**, *34*, 276–281.
- 548 (15) Cundy, C. S.; Cox, P. A. The hydrothermal synthesis of
549 zeolites: Precursors, intermediates and reaction mechanism. *Micro-*
550 *porous Mesoporous Mater.* **2005**, *82*, 1–78.
- 551 (16) Liu, Z.; Zhu, J.; Wakihara, T.; Okubo, T. Ultrafast synthesis of
552 zeolites: breakthrough, progress and perspective. *Inorg. Chem. Front.*
553 **2019**, *6*, 14–31.
- 554 (17) Tan, C.; Liu, Z.; Yonezawa, Y.; Sukenaga, S.; Ando, M.;
555 Shibata, H.; Sasaki, Y.; Okubo, T.; Wakihara, T. Unique crystallization
556 behavior in zeolite synthesis under external high pressures. *Chem.*
557 *Commun.* **2020**, *56*, 2811–2814.
- 558 (18) Davis, M. E. Zeolites from a materials chemistry perspective.
559 *Chem. Mater.* **2014**, *26*, 239–245.
- 560 (19) Burton, A. W.; Zones, S. I.; Elomari, S. The chemistry of phase
561 selectivity in the synthesis of high-silica zeolites. *Curr. Opin. Colloid*
562 *Interface Sci.* **2005**, *10*, 211–219.
- 563 (20) Burton, A. W.; Zones, S. I. Organic molecules in zeolite
564 synthesis: their preparation and structure-directing effects. *Stud. Surf.*
565 *Sci. Catal.* **2007**, *168*, 137–179.
- 566 (21) Rimer, J. D.; Kumar, M.; Li, R.; Lupulescu, A. I.; Oleksiak, M.
567 D. Tailoring the physicochemical properties of zeolite catalysts. *Catal.*
568 *Sci. Technol.* **2014**, *4*, 3762–3771.
- 569 (22) Olafson, K. N.; Li, R.; Alamani, B. G.; Rimer, J. D. Engineering
570 crystal modifiers: bridging classical and nonclassical crystallization.
571 *Chem. Mater.* **2016**, *28*, 8453–8465.
- 572 (23) Zhang, X.; Liu, D.; Xu, D.; Asahina, S.; Cychosz, K. A.;
573 Agrawal, K. V.; Al Wahedi, Y.; Bhan, A.; Al Hashimi, S.; Terasaki, O.;
574 Thommes, M.; Tsapatsis, M. Synthesis of self-pillared zeolite
575 nanosheets by repetitive branching. *Science* **2012**, *336*, 1684–1687.
- 576 (24) García-Martínez, J.; Xiao, C.; Cychosz, K. A.; Li, K.; Wan, W.;
577 Zou, X.; Thommes, M. Evidence of intracrystalline mesostructured
578 porosity in zeolites by advanced gas sorption, electron tomography
579 and rotation electron diffraction. *ChemCatChem* **2014**, *6*, 3110–3115.
- 580 (25) Linares, N.; Jardim, E. O.; Sachse, A.; Serrano, E.; García-
581 Martínez, J. The Energetics of surfactant-templating of zeolites.
582 *Angew. Chem., Int. Ed.* **2018**, *57*, 8724–8728.
- 583 (26) Peng, C.; Liu, Z.; Yonezawa, Y.; Linares, N.; Yanaba, Y.;
584 Trujillo, C. A.; Okubo, T.; Matsumoto, T.; García-Martínez, J.;
585 Wakihara, T. Testing the limits of zeolite structural flexibility: ultrafast
586 introduction of mesoporosity in zeolites. *J. Mater. Chem. A* **2020**, *8*,
587 735–742.
- 588 (27) Meynen, V.; Cool, P.; Vansant, E. F. Verified syntheses of
589 mesoporous materials. *Microporous Mesoporous Mater.* **2009**, *125*,
590 170–223.
- 591 (28) Thommes, M.; Cychosz, K. A. Physical adsorption character-
592 ization of nanoporous materials: Progress and challenges. *Adsorption*
593 **2014**, *20*, 233–250.
- (29) Cychosz, K. A.; Guillet-Nicolas, R.; García-Martínez, J.;
594 Thommes, M. Recent advances in the textural characterization of
595 hierarchically structured nanoporous materials. *Chem. Soc. Rev.* **2017**,
596 *46*, 389–414. 597
- (30) Mendoza-Castro, M. J.; Serrano, E.; Linares, N.; García-
598 Martínez, J. Surfactant-templated zeolites: from thermodynamics to
599 direct observation. *Adv. Mater. Interfaces* **2021**, *8*, No. 2001388. 600
- (31) Bini, R.; Ceppatelli, M.; Citroni, M.; Schettino, V. From simple
601 to complex and backwards. Chemical reactions under very high
602 pressure. *Chem. Phys.* **2012**, *398*, 262–268. 603
- (32) Fournier, R. O.; Rowe, J. J. The solubility of amorphous silica
604 in water at high temperatures and high pressures. *Am. Mineral.* **1977**,
605 *62*, 1052–1056. 606
- (33) Dawson, D. R.; Offen, H. W.; Nicoli, D. F. Pressure effects on
607 micellar size. *J. Colloid Interface Sci.* **1981**, *81*, 396–401. 608
- (34) Fisch, M. R.; Benedek, G. B. The effect of hydrostatic pressure
609 on micelle size and crystallization. *J. Chem. Phys.* **1986**, *85*, 553–558. 610
- (35) Nishikido, N.; Shinozaki, M.; Sugihara, G.; Tanaka, M.;
611 Kaneshina, S. A study on the micelle formation of surfactants in
612 aqueous solutions under high pressure by laser light-scattering
613 technique. *J. Colloid Interface Sci.* **1980**, *74*, 474–482. 614
- (36) Dawson, D. R.; Offen, H. W.; Nicoli, D. F. Pressure effects on
615 micellar size. *J. Colloid Interface Sci.* **1981**, *81*, 396–401. 616
- (37) Kresge, C. T.; Leonowicz, M. E.; Roth, W. J.; Vartuli, J. C.;
617 Beck, J. S. Ordered mesoporous molecular sieves synthesized by a
618 liquid-crystal template mechanism. *Nature* **1992**, *359*, 710–712. 619
- (38) Beck, J. S.; Vartuli, J. C.; Roth, W. J.; Leonowicz, M. E.; Kresge,
620 C. T.; Schmitt, K. D.; Chu, C. T. W.; Olson, D. H.; Sheppard, E. W.;
621 Et, A. A new family of mesoporous molecular sieves prepared with
622 liquid crystal templates. *J. Am. Chem. Soc.* **1992**, *114*, 10834–10843. 623
- (39) Mokaya, R. Influence of pore wall thickness on the steam
624 stability of Al-grafted MCM-41. *Chem. Commun.* **2001**, *7*, 633–634. 625
- (40) Cheng, C.; Chou, S.; Cheng, P.; Cheng, H.; Yak, H. Control of
626 Wall Thickness and Extraordinarily High Hydrothermal Stability of
627 Nanoporous MCM-41 Silica. *J. Chin. Chem. Soc.* **2007**, *54*, 35–40. 628